Temporary Recovery of the Defect Responsible for Light- and Elevated Temperature-Induced Degradation: Insights Into the Physical Mechanisms Behind LeTID

Wolfram Kwapil, Jonas Schön, Tim Niewelt, and Martin C. Schubert

***Abstract*—The effect of light- and elevated temperature-induced degradation (LeTID) can be nonpermanently reversed by charge carrier injection below the degradation temperature (commonly used degradation temperatures are above ∼70 °C). In this study, we show that the rate of temporary recovery depends strongly on the excess carrier density. We observe that the order of the reaction changes from pseudo-zero to first with increasing injection. The rate decreases slightly with increasing temperature. Since the samples can go through multiple degradation/recovery cycles without distinct changes in the degradation kinetics, the experimentally accessible recovered and degraded states are interpreted as manifestations of the equilibrium concentrations of the defect responsible for LeTID at different temperatures. Based on our observations, we argue that the process underlying LeTID degradation is the dissociation of a precursor rather than an association of two or more components. In light of the relation between LeTID susceptibility and bulk hydrogen concentration, we hypothesize that the LeTID precursor dissociates into the LeTID defect and monatomic hydrogen. Numerical simulations of the coupled rate equations including hydrogen interactions well reproduce the experimental observations; according to these results, the presence of a sink for the atomic hydrogen such as dopant atoms is paramount for the LeTID degradation.**

***Index Terms*—Degradation, Defect reactions, light- and elevated temperature-induced degradation (LeTID), model, silicon defects.**

I. Introduction

AFTER the first description of the phenomenon later termed light- and elevated temperature-induced degradation (LeTID) [1], extensive research has been conducted on the influences determining the LeTID extent and kinetics. Noting the

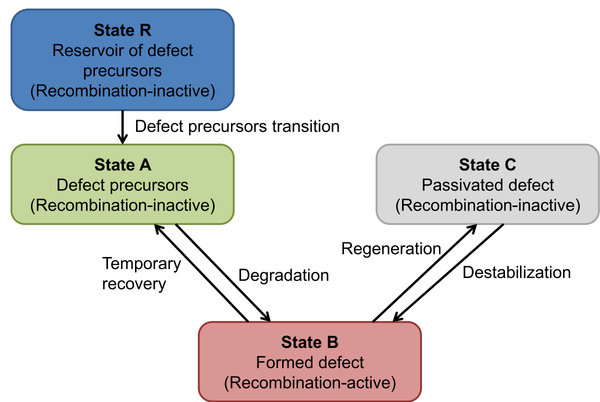

Fig. 1. Sketch of the states and transitions of the LeTID defect, adapted from [18].

similarity between LeTID and the boron-oxygen-(BO)-related degradation and regeneration in the carrier lifetime evolution, a three-stage model originally intended for the BO-defect evolution [2] was adopted for LeTID (for illustration see Fig. 1) [3]: After the firing process with rapid heating and cooling ramps [4], most LeTID defects are in an inactive precursory state *A*, allowing for high carrier lifetimes (and good module performance). The LeTID defect is formed and the system moves into the degraded state *B* by carrier injection at temperatures above an apparent “threshold temperature” T_{thr} of around 50–60 °C severely decreasing the carrier lifetime to values as low as several tens of microseconds. Hence, with regard to (PERC) modules, significant performance losses can be expected especially in warm, sunny regions if no counter measures are taken [5]. Upon prolonged exposure to degradation conditions, the system reaches the regenerated state *C* in which the LeTID defect appears to be permanently deactivated.

The LeTID phenomenon has been observed on all different material types ranging from p-type multicrystalline silicon [1], Cz silicon [6], [7], cast-mono silicon [8], and even float-zone silicon [9], [10] to various n-type materials [8], [11]–[13]. All the materials have in common that in order to be susceptible to LeTID, a during the firing step (or hydrogen must be introduced otherwise [14,15]), and that the LeTID, and that the LeTID extent is highly sensitive to the peak firing temperature. The

Manuscript received May 25, 2020; revised July 15, 2020 and August 26, 2020; accepted September 1, 2020. Date of publication September 30, 2020; date of current version October 21, 2020. This work was supported in part by the German Federal Ministry for Economic Affairs and Energy (BMWi) and by the Industry Partners under Grant 0324204A and Grant 0324204C, and in part by under Grant 03EE1052B. *(Corresponding author: Wolfram Kwapil.)*

Wolfram Kwapil, Jonas Schön, and Tim Niewelt are with the Freiburg Material Research Centre of the University of Freiburg, 79104 Freiburg, Germany, and also with the Fraunhofer Institute for Solar Energy Systems ISE, 79110 Freiburg, Germany (e-mail: wolfram.kwapil@ise.fraunhofer.de; jonas.schoen@ise.fraunhofer.de; tim.niewelt@ise.fraunhofer.de).

Martin C. Schubert is with the Fraunhofer Institute for Solar Energy Systems ISE, 79110 Freiburg, Germany (e-mail: martin.schubert@ise.fraunhofer.de).

Color versions of one or more of the figures in this article are available online at https://ieeexplore.ieee.org.

Digital Object Identifier 10.1109/JPHOTOV.2020.3025240

This work is licensed under a Creative Commons Attribution 4.0 License. For more information, see https://creativecommons.org/licenses/by/4.0/

LeTID kinetics appear to depend on the material type [8]–[10]. Whether this is a result of the difference in the crystalline structure, the difference in the present impurities, or whether this indicates a fundamental difference in the LeTID defect itself has not been clarified yet. However, it seems very unlikely that the many commonalities with regard to the influences on the LeTID behavior should be caused by very different LeTID defects.

A wide parameter range of elevated temperatures and injection conditions in various combinations has been studied in the past. In a very early study, Luka *et al*. [14] demonstrated that the efficiency of LeTID-degraded solar cells could be partially restored by annealing in the dark at around 200 °C; the cells could then be redegraded. Due to the apparent similarity to BO-related degradation and nonpermanent recovery, which is explained by reversible changes between two equilibrium states [2], it first seemed obvious that for LeTID, a comparable mechanism is at play, i.e., the recovery at around 200 °C represents the transition from state *B* into the initial state *A* [3].

However, later works showed the intriguing complexity of the influences of dark anneals (DA) on LeTID: First, detailed investigations revealed that the participation of excess carriers is not always necessary to provoke degradation and regeneration; the same cycle also occurs during DA at an elevated temperature within a certain range around 175 °C [6]. Samples treated in this way—irrespective of the degradation/regeneration stage reached during DA—are susceptible to another degradation/regeneration-cycle if LeTID conditions including excess carriers are applied afterward [15]. Second, DAs change the LeTID degradation/regeneration kinetics in later cycles in a highly complex manner [16], [17].

For the context of this work, it is most relevant that the DA/LeTID cycles cannot be repeated indefinitely, as the degradation extent monotonically decreases with each cycle, at least for DAs at ∼230 °C [18]. For example, the drop in carrier lifetime due to LeTID after five DA/LeTID cycles is only half of the initial difference. It was concluded that the LeTID defect moves from state *A* into states *B* and *C*, but during the DA, state *A* is replenished from a reservoir state *R*, see Fig. 1. Hence, the mechanism during DA is not the transition from state *B* to state *A* as initially assumed.

In several publications, it was mentioned that the second type of recovery from the degraded state can be provoked by injecting carriers at room temperature [9], [19], [20]. This "recovery" is not permanent and the degradation-recovery cycle can be repeated [19].

In the present contribution, we investigate the physical properties of this low-temperature temporary recovery (TR) reaction after LeTID in more detail. We will argue that the TR constitutes the backward transition from state *B* into state *A*. Since all experimental observations are always the result of the superposition of forward and backward reactions, we gain valuable information about the general physical mechanism behind LeTID by taking the $B \rightarrow A$ transition into account.

It is a common understanding that hydrogen plays an important role for the LeTID defect reaction [4], [9], [12], [13], [20]–[26]. Therefore, we propose a defect reaction involving hydrogen that could explain LeTID. In numerical simulations, we couple the LeTID degradation and TR reactions with the hydrogen reactions and explore the parameter range allowing for reproducing experimental observations, explicitly considering known hydrogen interactions in the temperature range of interest (i.e., change in charge states, hydrogen molecule formation and dissociation, pairing with dopant atoms, and formation of stable dimers [27]).

II. Experimental

The experiments in this study are similar to the approach used for studying the degradation kinetics in [28]. They were conducted on p-type industrial multicrystalline Si PERC solar cells, which were intentionally processed by an industrial partner to be highly susceptible to LeTID. The typical commercial high-performance mc-Si material had a base resistivity of 1.6 Ωcm. The full square solar cells were diced into quarters in order to increase the accessible current density range which was experimentally restricted by the current limitation of the power supply (10 A).

Note that—judging by the differences in the degradation and regeneration rates between different materials—the following results on the rate of the TR may differ for other materials, such as B-doped Cz-Si or FZ-Si. As the degradation and regeneration rates follow the same general trends with regard to injection- and temperature-dependence regardless of the (p-type) material, however, we assume the same general trends for the TR apply to monocrystalline materials, too.

Degradation and TR were performed on a hot plate by applying a constant voltage bias in the dark to the solar cells and monitoring the evolution of the current overtime by logging the voltage drop across a serially connected precision resistor of small resistivity. In this way, the excess carrier density at the pn-junction was kept in a narrow range defined by the set voltage during the entire time.

The bias voltage V_a being held constant by the power supply, the measured current change is entirely due to a change in the dark saturation current I_0, assuming a one-diode model

$$I\left(t\right) = I_0\ \left(t\right)\left(\exp\left(\frac{V_a}{k_B T}\right) - 1\right). \quad (1)$$

where k_B signifies the Boltzmann constant and T is the temperature.

The saturation current can be understood as a recombination parameter (for an instructive discussion, see e.g. [29]) which is proportional to the LeTID defect density in our case. Therefore, the measured current change directly translates into a change in LeTID defect concentration, assuming that this is the only defect undergoing some transformation.

If not indicated otherwise, all samples were degraded under the same conditions prior to TR, i.e., by applying a constant bias of 550 mV at a constant temperature of 75 °C for ∼20 h. This resulted in a degradation extent close to the maximum as indicated by experiments on sister samples. We chose to stop degradation shortly before its maximum to avoid the significant contribution of the regeneration reaction to our experiment.

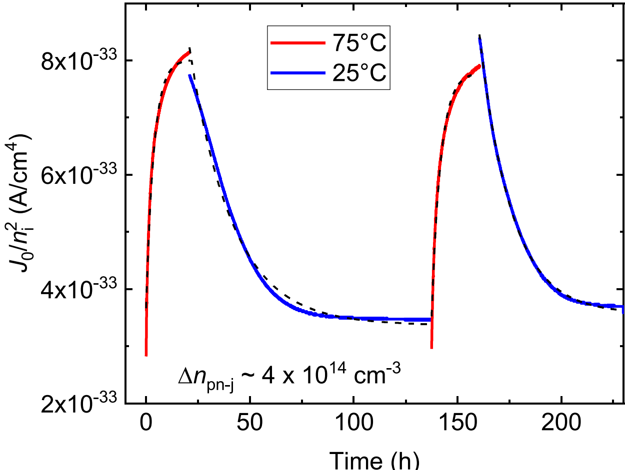

Fig. 2. J_0 normalized by $n_i{}^2$ of the first two degradation (red curves)/TR (blue curves) cycles. The dashed lines indicate the exponential fits according to (2).

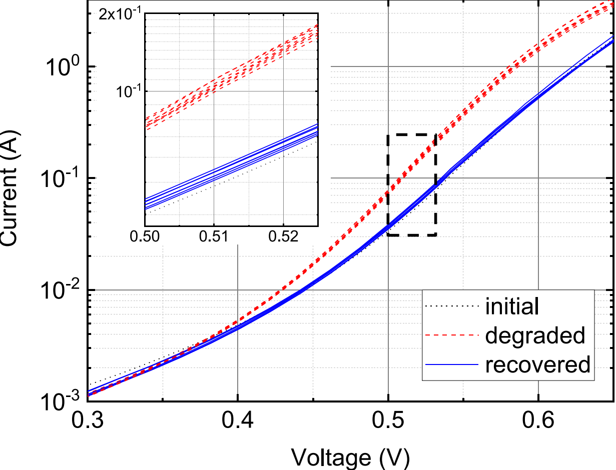

Fig. 3. Dark *I–V* curves of one quarter of a mc-Si PERC solar cell, subjected to cycling through degradation at 543 mV applied bias, 75 °C for 24 h ("degraded") and TR) at 652 mV, 25 °C for >48 h ("recovered") for eight times. The inset zooms into a part of the IV-range used for the determination of the J_{01} value indicated by the dashed box.

Afterward, the TR reaction was investigated by varying the injection conditions at 25 °C as well as by varying the temperature at the same excess carrier density of $\sim 1 \times 10^{15}$ cm^{-3}. To account for the temperature dependence of $\Delta n_{\text{pn-j}}$, the bias was adjusted accordingly. Set voltages V_a in the range between 600 and 700 mV were investigated. Due to the very high current flows especially at increased V_a, a significant voltage drop due to the series resistance, which was in the order of 0.6 Ωcm² for all solar cells, had to be taken into account.

III. Temporary Recovery

In order to demonstrate the fundamental difference between the TR and the recovery observed during DA, one of the solar cell quarters was subjected to a cycling experiment of repeated degradation and TR. The two alternated steps were 1) LeTID degradation (75 °C, 543 mV applied bias corresponding to $\Delta n_{\text{pn-j}} \sim 4 \times 10^{14}$ cm^{-3}) for 24 h (thus, reaching almost the maximum degradation extent) and 2) TR (25 °C, 652 mV corresponding to the same $\Delta n_{\text{pn-j}}$) for more than 48 h, until the current reached saturation. As an example, Fig. 2 shows the first two cycles. The cycling was repeated eight times.

The solar cell parameters in the degraded and annihilated state did not change significantly during cycling, as demonstrated in Fig. 3. In particular, the degradation extent, manifested in the J_{01} part of the *IV* curves, decreased only slightly during the repetitions, which is probably a result of the regeneration reaction progressing in parallel to the degradation. However, the decrease between cycles is much smaller than the one observed during DA cycling.

With the applied voltage settings, the measured current values both during degradation and TR follow an exponential behavior as a result of the change in I_0 according to the equation

$$I_0(t) = I_{0,\text{final}} + (I_{0,\text{init}} - I_{0,\text{final}}) \exp(-k_{ij} t), \quad (2)$$

where $I_{0,\text{init}}$ and $I_{0,\text{final}}$ are the initial and the final (equilibrium) value of I_0, respectively, and k_{ij} stands for the degradation rate coefficient k_{AB} and the TR rate coefficient k_{BA}. Fig. 4 shows k_{AB} and k_{BA} during repeated cycling, extracted via fits to (2) (see Fig. 2). It appears that the degradation rate coefficient decreases slightly with each repetition, whereas the TR rate coefficient increases. After several cycles, both rates seem to saturate. It should be noted that the deviations between the rate coefficients are within or close to the measurement uncertainty as determined by error propagation [28]. Hence, we conclude that cycling has only a small impact on LeTID kinetics.

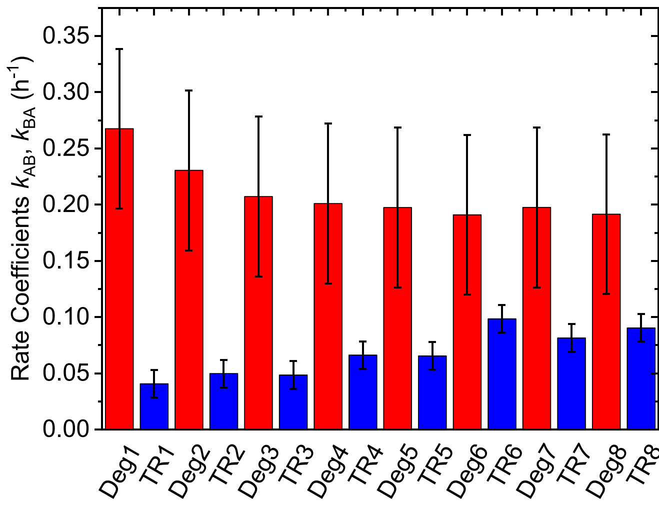

Fig. 4. Rate coefficients k_{AB} and k_{BA} resulting from single exponential fits to the current change during degradation ("Deg" in red) and "TR" (in blue), respectively, during cycling.

In Fig. 5, electroluminescence images of one solar cell quarter in the initial state (a), after degradation at 75 °C for ∼20 h at 543 mV applied bias (b), and after complete TR at 25 °C and 700 mV applied bias (c) are displayed. They are good examples of the observations obtained for different degradation and

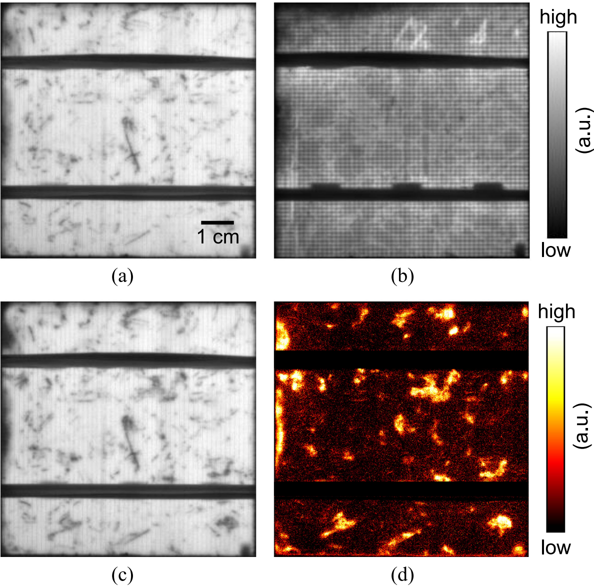

Fig. 5. Electroluminescence images of a quarter of a solar cell (a) before degradation, (b) after degradation, (c) after complete TR, (d) difference image of (a)–(c). All images were acquired at room temperature at a bias of 620 mV; images (a) and (c) have the same scaling.

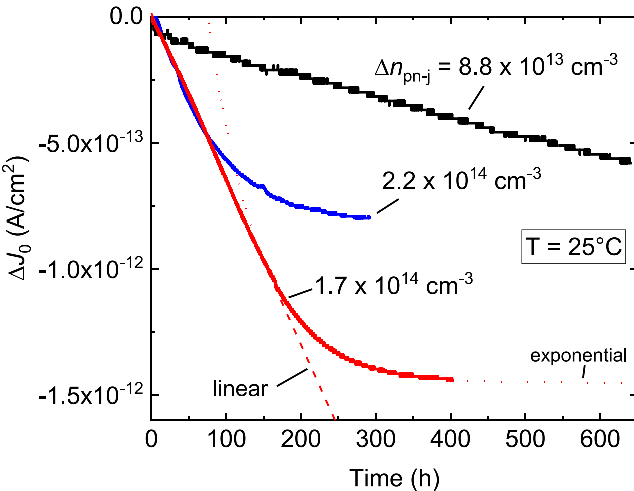

Fig. 6. Temporal evolution of J_0 at different low constant forward biases after having degraded the samples at 75 °C and 550 mV for ~20 h. The dashed and dotted lines indicate linear and single exponential fits, respectively, to the measurement at $\Delta n_{\text{pn-j}} = 1.7 \times 10^{14}$ cm^{-3}.

recovery conditions. All images were captured at 25 °C under a forward bias of 620 mV. As already shown in previous studies [14], [30], in highly LeTID susceptible samples, the degradation is most dominant inside the grains; grain boundaries are brighter in the degraded state due to a lower defect concentration [see Fig. 5(b)]. In addition, the degradation extent seems to differ slightly between different grains, possibly due to the influence of the grain orientation. The influence of the crystalline structure is overlaid by the pattern of the PERC contact openings, parallel to the busbars at the solar cell rear, which have a beneficial effect. Note that the apparent checkerboard pattern is an effect of the fingers at the front.

A comparison of the defect distribution in the initial state Fig. 5(a) with the one after a complete degradation/recovery cycle (c) indicates that the recovery is not fully accomplished. For illustration, Fig. 5(d) displays the difference image between these states. The significant difference values in dislocation clusters indicate that particularly in these regions the LeTID defect remains active after TR.

In summary, our interpretation of these observations is that, by switching between 25 and 75 °C and injecting charge carriers, the recombination-active LeTID defect switches between its equilibrium concentrations, being small at room temperature and high at 75 °C. It means that during TR, the transition from state B (recombination-active) to state A (precursor state) dominates. The high repeatability during cycling suggests that no additional precursors are formed from the reservoir (transition $R \rightarrow A$) and the regeneration (transition $B \rightarrow C$) is insignificant under these experimental conditions.

A. Dependence on Excess Carrier Density

The influence of the charge carrier density on the kinetics of the TR reaction is very strong. Fig. 6 displays the variation in J_0, calculated by assuming a simple one-diode model, for the lowest applied biases in this study. Our experiments indicate that the type of reaction changes between low and intermediate injection. For an excess carrier density $\Delta n_{\text{pn-j}}$ of $\sim 8.8 \times 10^{13}$ cm^{-3}, the defect deactivation over time is a linear function over the observed period. At $\Delta n_{\text{pn-j}}$ of around 1×10^{14} cm^{-3}, the TR initially also progresses linearly, but with a higher reaction rate. The TR then changes to an exponential behavior when the LeTID defect is almost completely annihilated. At higher injection densities, the entire curves can be described by single exponential functions; hence, the exponential part becomes dominant, so that an initial linear part cannot be discerned any more.

At present, it is unclear whether the linearity at very low injection is characteristic for the reaction (indicating pseudo-zero order at low Δn), or whether it is an effect of the geometry of carrier injection by means of applying a forward bias in the dark. If the diffusion length of electrons L_e is in the order of the solar cell thickness W or below (in our solar cells, this would be the case if the effective carrier lifetime $<\sim 10$ μs), the electron distribution along the depth is inhomogeneous to a significant extent. Hence, if $L < W$ in the degraded state, we expect that the TR progresses with different speeds along the wafer depth at the beginning. As the recovery proceeds and the diffusion length increases, the electron distribution along the wafer depth levelizes. The fact that we observe a linear part only at sufficiently low injection can be explained by the high temporal resolution in this case. This hypothesis could be tested by injecting carriers more homogeneously along the depth via illumination with long wavelength light.

Due to the uncertainty, Fig. 7 displays only the rate coefficients k_{BA} of the TR at 25 °C obtained by fitting to the exponential parts of the measured curves.

The first-order rate coefficients k_{BA} depend superlinearly on the excess carrier density, with the best fit indicating proportionality to $\Delta n^{1.71}$, which is close to Δn^2. This could suggest that

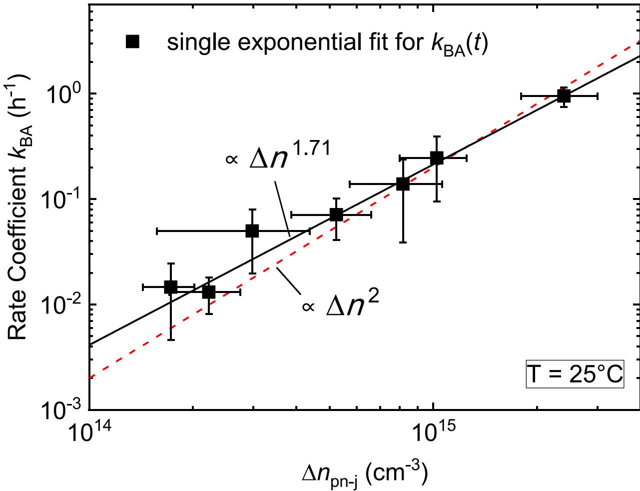

Fig. 7. TR rate coefficient k_{BA} of the exponential part of the measurements versus the excess carrier density at the pn junction. The best fit with proportionality to $\Delta n^{1.71}$ (black straight line) is displayed along with proportionality to Δn^2 (red dashed line) for comparison.

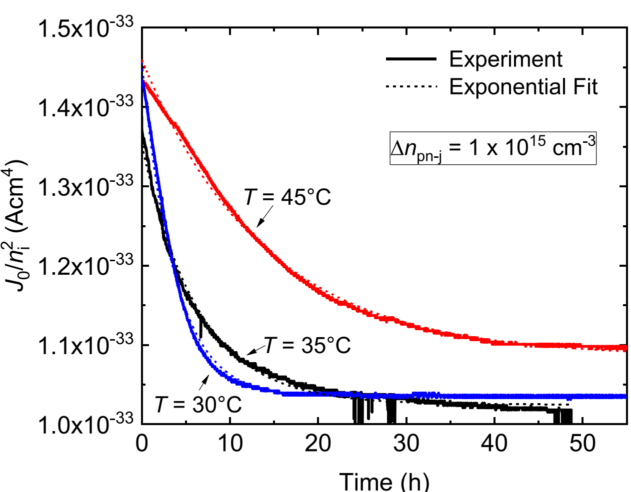

Fig. 8. Temporal evolution of J_0 normalized by $n_i{}^2$ by applying a constant bias at different temperatures after having degraded the samples at 75 °C and 550 mV for ~20 h. At the used injection, the measured decrease (straight lines) can be fitted with single exponential functions (dashed lines).

the TR reaction, i.e., the reformation of the precursor, needs two electrons per LeTID defect.

B. Dependence on Temperature

The temperature dependence of the recovery reaction was investigated by aiming to obtain the same $\Delta n_{\mathrm{pn\text{-}j}}$ of 1×10^{15} cm^{-3} for all the different temperatures. At this injection, single exponential function fits were performed and always showed satisfactory agreement, as demonstrated in Fig. 8.

Interestingly, the dependence of the recovery rate coefficient k_{BA} on the temperature appears to be weak. Between 25 and 50 °C, k_{BA} even seems to decrease slightly with increasing T, see Figs. 8 and 9 (note the different scaling compared to Fig. 7).

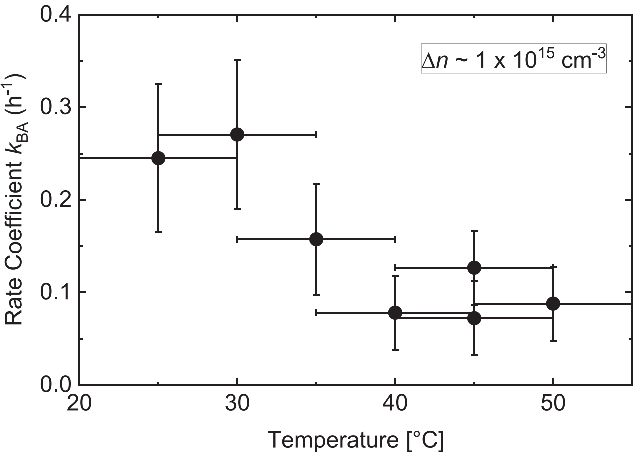

Fig. 9. TR rate coefficient k_{BA} versus temperature at the same excess carrier density.

The decrease of k_{BA} with increasing T contrasts with the usual expectation that a reaction is faster with higher temperature.

It is possible that the permanent regeneration reaction starts to play a role with increasing T. Occurrence of an additional competing transition reaction is not covered by the approach of fitting single functions to the data and would, therefore, distort the result. For a temperature of 55 °C and above, we are certain that the permanent regeneration ($B \to C$) begins to dominate, hence these measurement points are not shown. However, both the TR reaction and the regeneration lead to a decrease in the LeTID defect concentration, which is the quantity observed in our experiment. With the activation energy of the regeneration reaction being clearly positive [17], [31], we would expect the rate to increase with increasing temperature regardless of which reaction is the dominating one.

The change of the solar cells' series resistance with temperature is not exactly known. In the data analysis, the measured series resistance R_s at room temperature was taken into account. It is reasonable to assume that R_s increases with increasing T, which would result in a reduction of the excess carrier injection with increasing temperature. The dependence of k_{BA} on injection being strong, even slight deviations in $\Delta n_{\mathrm{pn\text{-}j}}$ would lead to significant changes in the TR rate. Hence, the observed T-dependence could be dominated by a resulting series resistance effect.

Since we cannot rule out the possibility that the experimental design interfered with our investigation of the temperature dependence, additional efforts, therefore, have to be undertaken in future studies to determine the exact activation energy of the TR reaction. Assuming the TR follows an Arrhenius-type reaction behavior, the activation energy is probably very small.

IV. Development of a Model Describing Degradation and TR

Analyzing the reaction kinetics can give valuable information about the mechanisms involved in the defect formation and, hence, also on the defect structure itself.

A. General Reactions and Equilibrium Concentrations

For the following deduction of a potential physical mechanism of LeTID, we make several simplifications. We start with the assumption that LeTID degradation and TR can be mainly explained each by a single-step process as opposed to a reaction chain, meaning that the LeTID precursor or the LeTID defect do not have to undergo any transformation or reconfiguration prior to the degradation or recovery reactions.

An important question is whether the defect formation—the degradation—is related to the *dissociation* of a LeTID precursor complex *Lp* (case I)

$$Lp \rightleftharpoons LD + Y \tag{3}$$

into the components *LD* (for LeTID Defect) and the unknown *Y*, where (at least) *LD* is highly recombination active (this proposal was also published in [32]), or to an *associative reaction* (case II)

$$Lp + Y \rightleftharpoons LD \tag{4}$$

or whether it is due to a (structural) *reformation* of a defect complex without any migration involved (case III)

$$Lp \rightleftharpoons LD. \tag{5}$$

The latter mechanism was proposed, for example, to be responsible for BO-related degradation and annealing [33]. There is no obvious reason speaking against such a mechanism for the case of LeTID and, therefore, it should be kept in mind for further investigations.

At present, however, we shall focus on the first two possibilities and discuss whether both, cases I and II, are equally likely. As outlined above, the LeTID *degradation* occurs above a certain apparent "threshold temperature" T_{thr}. On the other hand, TR of degraded samples happens below the degradation temperature and represents the reverse reaction of the degradation. If the LeTID defect formation were an association of two precursors (case II), it would mean that the recovery would be related to the dissociation of the LeTID defect, which would happen at a lower temperature than the association. While not impossible this disagrees with the usual experience that complexes tend to associate at lower temperature and dissociate at higher temperature.

This argument can be investigated in more depth by analyzing the equilibrium LeTID defect concentration [*LD*] and the activation energies as estimated from experiments.

Let us suppose that the temporal evolution of [*LD*] follows the simple reaction rate equation

$$\frac{d\,[LD]}{dt} = k_{\mathrm{AB}}\,[Lp] - k_{\mathrm{BA}}\,[LD]\,[Y] \tag{6}$$

with [*Lp*] denoting the LeTID precursor concentration, which is a complex of the LeTID defect *LD* and some unknown component *Y*, and k_{AB} and k_{BA} denote the reaction rate coefficients of the degradation and recovery, respectively. Both are here assumed to exhibit the common Arrhenius-like behavior with $k_i = k_{i,0}\,\exp(-E_{\mathrm{a,i}}/k_{\mathrm{B}}T)$. In (6), the reaction of case I is described; for case II, the concentration [*Y*] would belong to the degradation term including k_{AB}.

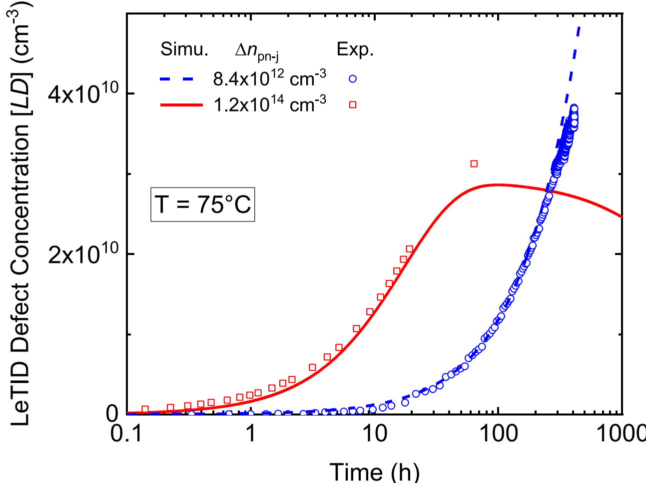

Fig. 10. Simulated degradation at two different injection conditions. Experimental results were taken from [28].

From (6), the equilibrium *LD* concentration is connected to the reaction rate coefficients by

$$[LD] = \frac{k_{\mathrm{AB}}\,[Lp]}{k_{\mathrm{BA}}\,[Y]}\,. \tag{7}$$

The measured activation energy for the degradation $E_{\mathrm{a,AB}}$ lies in the order of ∼0.9–1.1 eV [34], [35], whereas $E_{\mathrm{a,BA}}$ has to be much smaller, say in the order of ∼0.1 eV, as indicated by our measurements of the temperature dependence (see Fig. 10). It can be easily shown that (6) and (7) predict the correct trends of the equilibrium [*LD*] concentration with temperature with these values.

Still, in principle, both reactions (cases I and II) could describe the LeTID defect formation. However, the activation energy for an associative reaction usually scales with the migration enthalpy of the more mobile component of the complex [36] (see, e.g., the formation of BH, which scales with the migration enthalpy of H^+). On the other hand, the activation energy of dissociation is related to the binding energy *plus* the migration enthalpy and is, therefore, expected to be higher [37]. If a dissociation/association reaction is at the base of LeTID (and not a structural reformation, case III), it can, therefore, be concluded that LeTID degradation is more likely provoked by a *dissociation* of some precursor defect due to its higher activation energy, rather than by an associative process.

The kinetic framework developed here would not support the existence of a sharp threshold temperature since the thermal activation of a reaction continually increases with *T*. The apparent "threshold" would rather be a result of very long timescales for degradation at lower temperature and a strong shift in the equilibrium LeTID defect concentration to lower values at lower temperature. The latter may be concealed by the influence of other background recombination mechanisms. Hence, we would expect to see LeTID also at temperatures not far above room temperature in LeTID-susceptible high-lifetime samples after very long times.

Next, the injection dependence of both the degradation as well as the recovery needs to be considered. As shown in a previous publication, the degradation rate increases linearly with Δn, which indicates that the LeTID precursor needs to catch an electron prior to dissociation [28]. On the other hand, the rate of TR depends very strongly on the injection, possibly on Δn^2 (see Fig. 7). This could mean that 1) both the LeTID defect *LD* and the second component *Y* have to catch an electron in order to re-form the LeTID precursor, or 2) either *LD* or *Y* possesses at least two defect states in the bandgap and catches two electrons. The following reaction holds:

$$Lp^{i+j+1} + e^- \rightleftharpoons LD^i + Y^j + 2e^- \tag{8}$$

with *i* and *j* being integers describing the charge states of the components, on which we have no information so far.

Of course, it is not unlikely that the reaction is more complex than implied by (8). For example, Bredemeier *et al*. [34] reported that degradation could only be parameterized by the superposition of two exponential functions in their experiments, which could indicate a two-step mechanism. This would necessitate an extended set of rate equations similar to (6), which could be easily implemented at the cost of more unknown parameters.

For the sake of simplicity, we try to keep the reactions as simple as possible in order to develop a numerical model.

B. Relation to Hydrogen

Since hydrogen incorporation is a prerequisite for the LeTID susceptibility of the samples, it must be considered that *Lp*, *LD,* and/or *Y* contain some form of hydrogen. It seems plausible that the highly complex behavior of the LeTID defect (e.g., the changed degradation kinetics after DA [38] or the extremely high sensitivity to the firing conditions [4]) may be related to the complicated interactions of hydrogen with charge carriers and defects [27], [39]. Therefore, an obvious first step is to incorporate (6) into the set of known hydrogen reactions.

Unfortunately, many details are still missing for accurate numerical simulations. Some of the most important open questions are following.

1) Without knowledge of the electron or hole capture cross sections and the defect level E_t of the LeTID defect *LD*, the relevant concentrations of all components are unknown.
2) Reaction paths and reaction rate coefficients for hydrogen interactions, in general, are highly uncertain. This is particularly true in the case of charge carrier excitation.
3) Besides the dopants (and *LD*), it appears likely that numerous traps interact with hydrogen which have not been considered in the simulations so far. For example, it is known that hydrogen passivates defects by tying up dangling bonds. For a recent review of hydrogen passivation, please see [40].

The following model is, therefore, mainly intended to provide a basis for the investigation of the physical nature of the LeTID defect. Despite its simplicity, it already allows the assessment of possible reaction channels to a certain degree. It can, therefore, help in designing experiments that are able to discriminate between different reactions and components.

The model is based on the hydrogen reactions published by Voronkov and Falster [27] and Hamer *et al*. [39]. A brief summary of its implementation can be found in Appendix A.

Equation (6) was added to the coupled rate equations for H, H_{2A}, HB, and H_{2C}, see Appendix A. The simplest approach for the LeTID reaction is to assume that component *Y* is monatomic H.

In addition, we assume, that both *LD* and *H* have to change charge state in order to exemplarily illustrate the consequences. According to the Sah–Shockley model, the changes in charge states necessary for the reactions to proceed depend on the defect levels and capture cross section ratios of *Lp*, *LD,* and *H*. For the latter, a parameter set using established defect levels [41] and an estimated guess for the capture cross section ratios based on a comparison to transition metal SRH parameters have been proposed by Sun *et al*. [42], which is used in the following. Vargas *et al*. [43] identified two possible defect levels of the LeTID defect *LD*; we assume the level in the upper band gap half in the following. We tested the model also assuming the level in the lower bandgap half, but the agreement between experiment and simulation was not as good. In an earlier publication [28], we showed that the LeTID degradation, i.e., the precursor dissociation, is likely triggered by a change in the charge state. The dependence of the degradation rate on the excess carrier density observed in our experiments can only be explained by a restricted range of SRH defect parameters of *Lp*. In the following, we assume the level to be 0.6 eV above the valence band (mid-gap, which means that the minority carrier capture cross section must be very small in order to have no impact on lifetime) and it has a capture cross section ratio of 1. These parameters are in the center of the possible combinations in the $E_t - k$ space [28]; other combinations work just as well.

V. Numerical Simulations

A first evaluation of the LeTID model was performed by checking the most prominent features of LeTID:

1) degradation and regeneration during injection of various concentrations of excess carriers at 75 °C;
2) degradation during DA at temperatures around 175 °C; and
3) TR from the degraded state at 25 °C with varying excess carrier concentrations.

The starting conditions in the simulation, i.e., the total hydrogen concentration and, in particular, the relative share of the different hydrogen complexes have a significant impact on the LeTID dynamics. In order to begin with a realistic estimation, a firing process was emulated: A total hydrogen concentration $[H]_{tot}$ of 1×10^{15} cm^{-3} (which is in the range of an expected concentration after a typical firing step [44]) was assumed to be in dissociated state at the peak temperature of 750 °C. The redistribution of hydrogen to the different complexes was simulated for a cool-down rate of 100 K/s down to room temperature. According to the simulations, starting with a higher peak temperature has no effect on the final distribution after cool-down. As a result, the large majority of H is present in the molecular form H_{2A} with a small amount of boron-hydrogen

TABLE I
SIMULATION PARAMETERS

Parameter	Value	Unit
$k_{AB,0}$	6×10^{11}	s^{-1}
$E_{a,AB}$	1.1	eV
$k_{BA,0}$	2.5×10^{-7}	cm^3s^{-1}
$E_{a,BA}$	0.1	eV
Trap level of Lp: $E_{t,Lp}$	E_V+0.6	eV
$\sigma_{e,Lp}/\sigma_{h,Lp}$	1	-
Trap level of LD: $E_{t,LD}$	E_C-0.3	eV
$\sigma_{e,LD}/\sigma_{h,LD}$	50	-
$\sigma_{e,LD}$	5×10^{-14}	cm^2

pairs HB. The concentrations of atomic hydrogen and the dimer H_{2C} are negligible. We believe that the LeTID precursors are formed during the firing and cool-down, but the formation path is unclear. It is likely that additional reactions take place; hence the LeTID dynamics were ignored in this first simulation step.

An important first result of the numerical simulation is that, even without knowing the concentrations of the participating components (atomic hydrogen, hydrogen complexes, LeTID precursor, and defect), our experimental observations can only be explained by a set of degradation and recovery rate coefficients within relatively narrow limits. This is due to the fact that the model needs to reproduce not only the experimentally observed rates of degradation and recovery but also reasonable equilibrium concentrations, which are defined by the ratio of k_{AB} and k_{BA} [see (7)]. Since the carrier lifetime difference between degraded and recovered (or initial) state can be very large (in extreme cases the minority carrier lifetime decreases from above 1 ms to several ten microseconds [9]), physically plausible LeTID defect parameters and concentrations are only found within a very restricted range of $k_{\mathrm{AB}}/k_{\mathrm{BA}}$ value pairs: In order to obtain the large difference in [LD] between 25 and 75 °C, $E_{\mathrm{a,AB}}$ and $E_{\mathrm{a,BA}}$ must differ by $\sim$1 eV $\pm$ $\sim$0.1 eV. We chose to use the measured degradation rates as fix points, see below. Depending on the chosen E_{a} values, the prefactors need to be adjusted and may vary about one order of magnitude around the tabulated values with still giving reasonable agreement to experiments.

The aim of the following paragraphs is to demonstrate that many of the experimental results can be consistently reproduced by our model with a single set of parameters.

As hydrogen is involved in all of the model equations, in which absolute concentrations are handled, we have to estimate the quantitative amount of LeTID precursors and LeTID defects in order to take into account the interactions with the other H complexes. Our approach for this quantification can be found in Appendix B.

Table I contains the parameters used in the following subsections which give satisfactory fits. It is worth having a brief look on the pre-exponential factors and activation energies of the reaction rate coefficients. The activation energy of the degradation was chosen to coincide with the value of 1.08 $\pm$ 0.05 eV given by Vargas *et al*. [35] for the case of degradation induced by dark annealing. The fact that other experiments tend to produce lower values (e.g., [34]) under illumination is reminiscent of Zundel's observations on the dissociation rates of HB-pairs [45]. The pre-exponential factor of the dissociation coefficient is called the attempt frequency, which usually scales with the phonon frequency in the order of $\sim10^{13}$ s^{-1}. Given the uncertainties, $k_{\mathrm{AB},0}$ is in good agreement with this value.

The recovery rate coefficient can be compared to the common approach of diffusion limitation [36] which for our case would read

$$k_{BA} \cong 4\pi \left(D_{LD^0} + D_{H^0}\right) a. \tag{9}$$

Here, $D_{\mathrm{LD}}{}^0$ and $D_{\mathrm{H}}{}^0$ stand for the diffusion coefficients of the reacting species, the LeTID defect and atomic hydrogen, and a is a capture radius, which is in the order of $\sim$2.5 Å if no Coulombic forces are in effect [37]. Equation (9) is dominated by the higher diffusivity. Unfortunately, the diffusivity of H^0 is not well known. H^0 can be found at bond-centered or at the tetrahedral interstitial (T) site. At least, $H^0{}_{\mathrm{T}}$ is known to be extremely fast, with activation energy in the order of 0.1 eV [46], [47], being in good accordance with the fit parameter.

In summary, the parameters describing the experimental results best do not conflict with physically plausible values.

We also tested the possibility that negatively charged atomic hydrogen reacts with the positively charged LeTID defect [i.e., possibility 2) for (8)]. In that case, we would expect the rate coefficient k_{BA} of the TR to be dominated by the diffusivity of H^-, whose migration enthalpy has been reported to lie in the range of 0.39–0.7 eV [39]. In addition, Coulombic interaction has to be taken into account in a manner similar to the interaction between dopant atoms and hydrogen (see Appendix A for HB pairs). According to Sun's model [42], the fraction of negatively charged hydrogen is very low in the investigated p-type silicon. This would significantly slow down the expected recovery reaction. Reasonable rates could still be achieved by assuming a capture cross section ratio larger than 0.05 for the donor level as proposed in [42].

However, even with these modifications, the fit results were not as good as those shown in the following for the TR reaction between two neutral species.

A. Degradation at 75 °C With Injection

As shown in Fig. 10, degradation under different injection conditions can be reproduced by our numerical model. The LeTID precursor concentration was assumed to be 5 $\times$ 10^{11} cm^{-3} for all measurements on cell level because the solar cells were processed together from the same material and, thus, feature the same LeTID susceptibility. The model predicts different equilibrium values for [*LD*] for different injection conditions, with higher $[LD]_{\mathrm{eq}}$ for lower injection. Following (7), this is mainly due to the ratio of the rate coefficients $k_{\mathrm{AB}}/k_{\mathrm{BA}}$, which overall gives proportionality with $1/\Delta n$. Published experimental results could be interpreted to support this statement [19]. However, in reality, the degradation often does not reach a plateau but transitions seamlessly into the regeneration phase ($B \rightarrow C$). It is, therefore, difficult to assess the equilibrium defect concentration experimentally.

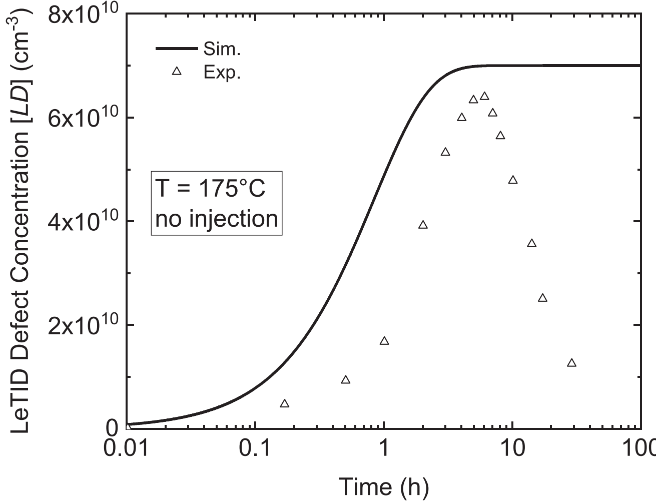

Fig. 11. Simulated degradation during Dark Anneal. Experimental results were taken from [6], Fig. 1(b).

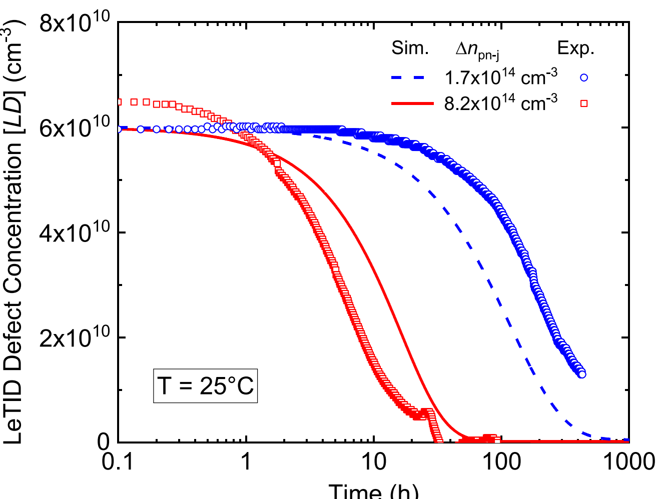

Fig. 12. Simulated recovery at two different injection conditions.

As shown for the higher injection in Fig. 10, the calculated LeTID defect concentration decreases slightly on longer timescales. This is a result of the slow formation of a stable dimer H_{2C}, which changes the equilibria between the different hydrogen complexes. According to the reaction proposed in [27], the formation of H_{2C} does not involve any electrons; hence it would not depend on the injection conditions. By contrast, experiments indicate that LeTID regeneration is driven by excess carriers as strongly as the degradation [17], [31], [48]. As an important result of the application of this model, we conclude that either the formation of the stable dimer does not follow the reaction pathway as proposed in [27], or regeneration is due to an entirely different reaction which is not yet part of our model.

B. Degradation at 175 °C in the Dark

For the experimental data, we took the normalized defect concentration as plotted in Fig. 1(b) in [6] and calculated the estimated LeTID defect concentration in the same way as described in Appendix B.

In the dark (no injection), degradation is observed at 175 °C, as demonstrated by the data of Chen *et al*. [6] shown in Fig. 11. According to our model, the equilibrium concentration of [*LD*] at increased temperatures must be much higher than assumed for our experiments under LeTID conditions (75 °C with excess carrier injection). Therefore, in order to have a good fit to experiments, the LeTID precursor concentration was adjusted to 8×10^{10} cm^{-3}, which we believe to be appropriate as the wafers were not processed in the same way as the solar cells.

At 175 °C, with the current parameter set the equilibrium between [*LD*] and [H_{2C}] is on the side of the LeTID defect, which would indicate a suppressed formation of the stable dimer even for much longer annealing steps. Hence, no regeneration occurs in the simulation in contradiction to experiments. Also, the regeneration observed in experiments prohibits evaluating the trends in equilibrium values.

Again, we reach the conclusion that either the reaction for H_{2C} formation is questionable, or we have to consider a further reaction for regeneration.

Nevertheless, considering the numerous uncertainties and assumptions, the degradation can be well described with the current parameter set irrespective of the temperature or injection conditions.

C. Temporary Recovery

While some experimental values of the degradation reaction rate coefficient k_{AB} exist, k_{BA} is difficult to determine due to its atypical temperature dependence. Hence, the values of $k_{\mathrm{BA},0}$ and $E_{\mathrm{a,BA}}$ should be considered rather uncertain. With the estimated values from Table I, a recovery reaction can be reproduced, as can be seen in Fig. 12.

As starting values for the simulation of the recovery, we simulated the distribution of the hydrogen between its different complexes after ~20 h at 75 °C and an injection of $\Delta n_{\mathrm{pn\text{-}j}} = 1 \times 10^{15}$ cm^{-3}. This injection is a reasonable approximation for the applied voltage in the experimental degradation process. The initial LeTID defect concentration was adjusted slightly in order to meet the measured values.

Although the simulation reproduces the trends regarding the injection dependence, the fits are not as good as for the degradation step; the simulation predicts recovery at a low injection of 1.7×10^{14} cm^{-3} to be faster than we observed in the experiments and slower for a higher injection of 8.2×10^{14} cm^{-3}. As a detailed analysis of the simulation results reveals, the reason for the differences of simulated and experimentally obtained kinetics is that at high injection the recovery reaction $LD^0 + H^0 \rightarrow Lp$ is limited by the supply of monatomic hydrogen at increased excess carrier concentration. This is a result of the assumed high LeTID precursor and defect concentration in relation to the total hydrogen concentration: the more LeTID defects there are the more monatomic hydrogen has to be present in order for the recovery reaction to proceed uninhibited. The

hydrogen atoms consumed by the LeTID defect for the formation of the LeTID precursor have to be resupplied by the other hydrogen complexes. If their dissociation rates are significantly lower than the LeTID recovery rate, the recovery reaction is inhibited. For our assumed parameter set, this was observed for higher injection.

Hence, from our hypothetical reaction, it follows that there should be a strong interplay between the LeTID precursor and the hydrogen concentration, the hydrogen complex reaction kinetics (e.g., dissociation of HB and H_{2A}), and the dynamics of the recovery reaction. We found that the misfit between experiment and simulation could be overcome by either increasing the total hydrogen concentration or decreasing the LeTID precursor concentration. The former would mean that the hydrogen concentration in the wafer is higher than expected from experiments [44]. As a consequence of the latter, the electron capture cross section σ_e would have to be larger than 5×10^{-14} cm^{-2} (and hence larger than that of all other defects) in order to explain observed very low lifetime values. Since our knowledge on both, the total hydrogen concentration in fired solar cells and the capture cross section of the LeTID defect, is limited, we think that both scenarios are possible.

VI. Discussion

Our model can provide valuable insight into the mechanisms behind LeTID by analyzing the simulation results in more detail. In order to understand the following statements, first of all, it is important to note that the solubility of monatomic hydrogen in silicon at room temperature or slightly above is extremely low. Extrapolation of high-temperature values as suggested by McQuaid even predicts zero solubility at room temperature [49]. At the same time, the diffusivity of atomic hydrogen remains relatively high. Thus, hydrogen will likely travel to potential binding partners or other sinks. It follows that the equilibrium between hydrogen complexes and atomic hydrogen is always on the side of the former.

To illustrate the consequences, let us assume for the moment that the LeTID defect precursor *Lp*, the defect *LD*, and atomic hydrogen were the only impurities present in the silicon matrix and that there were no other reactions involving hydrogen. In equilibrium at room temperature, the concentration of *Lp* would dominate. By increasing the temperature (and injecting charge carriers), *Lp* dissociates into the same amounts of *LD* and atomic *H*. The dissociation stops when the solubility limit of the latter is reached, which is at a very low concentration. Hence, in this hypothetical situation, the dissociation of the precursor complex would be suppressed. The degradation would stop long before it would have an impact on the carrier lifetime. However, in reality, atomic hydrogen is a highly reactive impurity. As a result, the fast sinking of the monatomic hydrogen in other complexes keeps $[H]_{\mathrm{at}}$ always at a low level. This acts as the driving force of the LeTID precursor dissociation and thus degradation. We conclude that a prerequisite for LeTID is the presence of effective sinks for atomic hydrogen. In principle, many different defects could act as such. In our simulated case, it is the HB-pairing reaction that effectively instigates the degradation: the boron atoms receive monatomic hydrogen both from hydrogen molecules and the LeTID precursor, until the system's equilibrium is reached. At room temperature and significant carrier injection, the reactions are reversed and the hydrogen released from the boron atoms together with the LeTID defects re-form the LeTID precursors. Only when equilibrium for [*Lp*] is reached in our model, the monatomic hydrogen continues to form hydrogen molecules H_{2A}.

As Fung *et al.* [23] showed by isochronal annealing experiments, there is a striking resemblance between the maximum [*LD*], the BO-defect regeneration rate (often used as an indicator for the hydrogen concentration), and [*HB*]. We note that also the temporal evolution of the LeTID degradation and [*HB*] during dark annealing at around 175 °C [27] are very similar. Fung *et al.*'s interpretation was that the HB pairs act as the hydrogen source and that the hydrogen was needed for the LeTID defect to form. In this picture, HB would be one part of the LeTID precursor. As explained above, we believe that a more natural explanation for the coincidence of LeTID defect and HB concentration as well as BO-defect regeneration rate is that the LeTID precursor and H_{2A} act as sources for monatomic hydrogen while B and possibly BO-defects act as sinks necessary for the reactions to continue.

In this theory, the availability and types of sinks would certainly have an influence on the degradation extent and possibly the degradation rate, depending on the nature of the reactions that are involved in the hydrogen complex formation. The sinks that are best controlled in silicon wafer processing are the dopant atoms. In a recent study, Hammann *et al.* [50] demonstrated that in otherwise similarly processed p-type FZ samples with different base resistivity, the maximum [*LD*] was much larger for samples with higher doping. This observation can directly be explained by our theory. In the same publication and in several previous works, e.g., by Chen *et al.* [12], [13], results on LeTID degradation in n-type Cz silicon were presented. In general, the LeTID degradation extent was significantly lower than in p-type silicon. This was associated with the lower solubility of H in n-type Si [12], [13]. We hypothesize, however, that the lower LeTID susceptibility could be a result of the different binding kinetics of HP pairs.

In this line of reasoning, the effect of anneals prior to degradation could be induced by the changes in the concentrations of the various hydrogen complexes, which, in turn, could change the reaction kinetics.

However, for a more thorough understanding of the various observations concerning the influences on LeTID kinetics, we would also have to take additional reactions into account, which we have not considered in our current model: the regeneration during prolonged application of degradation conditions, and an additional reaction explaining the formation of the LeTID precursor species from a reservoir at elevated temperatures as postulated by Fung *et al.* [18]. Up to date, the fundamental mechanisms behind the regeneration and the precursor replenishment from a reservoir are unclear. It is certain, however, that they affect the LeTID degradation/recovery kinetics by providing additional reaction channels.

Finally, we would like to repeat that we cannot rule out the possibility that LeTID degradation and recovery is due to the structural reformation of an impurity complex (case III).

VII. Conclusion

We investigated the TR of the LeTID defect, which occurs when charge carriers are injected around room temperature into samples that had previously been degraded under LeTID conditions. We found that the recovery rate increases strongly with increasing injection and decreases slightly with increasing temperature.

The nonpermanent recovery can be seen as the reverse reaction to LeTID degradation because the sample can be degraded and recovered several times without significant changes in the apparent defect distribution and reaction kinetics. From an analysis of the expected equilibrium concentrations of the LeTID defect in dependence of the degradation and recovery rates, we conclude that the degradation (LeTID defect formation) is probably due to a dissociation of a precursor complex. The recovery can then be explained to be an association of the LeTID defect with another, *a priori* unknown component. Another possibility is that the degradation and recovery are caused by the structural reformation of a defect complex under different temperature-injection conditions, similar to the model recently proposed for the activation of the BO-related defect.

We show that —if we assume this component to be atomic hydrogen—a numerical model of the hydrogen dynamics together with an equation describing the LeTID defect can reproduce many of the experimental observations, namely the injection-dependent degradation and recovery and the degradation due to annealing in the dark. According to our theory, the driving force behind LeTID is the presence of a binding partner or sink for the atomic hydrogen. Further work is needed to elucidate the interacting species forming *Lp* and *LD*.

Appendix

A. Implementation of the Hydrogen Reactions

It is common understanding [51], [52] that the majority of hydrogen atoms in standard p-type Si are present in two forms: either as hydrogen molecules H_2 (to follow the notation from [27], it will be called "H_{2A}" in the following), or bound to boron atoms to form HB-pairs. Besides the molecular form, another hydrogen dimer is presumed to exist (denoted "H_{2C}"), which is more stable than H_{2A} but forms only very slowly [27]. The solubility and, hence, the concentration of highly reactive monatomic hydrogen is relatively low in the temperature range typical for LeTID or BO regeneration [51]. Depending on the temperature and injection conditions, this monatomic hydrogen can be positively or negatively charged or electrically neutral. When the temperature and/or excess carrier concentrations are changed, the distribution of charge states of the monatomic hydrogen as well as the different complexes with levels in the silicon band gap can be assumed to adapt instantly. A new equilibrium between the monatomic form and the multiple hydrogen complexes establishes on longer timescales.

The following notions about hydrogen reactions are taken from Voronkov and Falster [27] and Hamer *et al*. [39], some of the parameter values were corrected using [44]. The hydrogen fractions in the different charge states were calculated according to Sun *et al*. [42]. The reaction pathways as described in [39] were left unchanged in our model even during charge carrier excitation. This is justified if excess carriers influence the reactions only by modifying the charge state fractions of the participating components and the charge states are explicitly considered in the reactions. Some support to the simplification of unchanged reaction pathways comes from the findings of Zundel *et al*. [45] who investigated the reactivation of the boron acceptors in hydrogenated silicon in the dark and under illumination at an increased temperature. At first glance, their results seemed to indicate that the reactivation reaction proceeds very differently depending on whether or not excess charge carriers are present during the anneal. However, the authors convincingly demonstrated that the reaction is dominated by the subsequent formation of hydrogen molecules (H_{2A}) after the HB-pair dissociation. Since the H_{2A} formation is more likely between monatomic species of different charge states preventing Coulombic repulsion, the illumination indirectly affects the HB dissociation. This experimental result can be qualitatively reproduced in Hamer's model used in the following.

The formation and dissociation of HB pairs is given by

$$\frac{d\left[HB\right]}{dt} = \frac{D_{H^+}q}{\varepsilon_{Si}kT}\left[H^+\right]\left[B^-\right] - \left(2.8\times10^{14}\mathrm{s}^{-1}\right) \times \exp\left(\frac{-1.28\mathrm{eV}}{kT}\right)\left[HB\right] \qquad \text{(A1)}$$

where $D_{\mathrm{H}+}$ signifies the diffusivity of positively charged atomic hydrogen (value taken from [53]) and $\varepsilon_{\mathrm{Si}}$ is the silicon dielectric permittivity. From this reaction, the equilibrium constant K

$$K = \frac{\left(2.8\times10^{14}\mathrm{s}^{-1}\right)\exp\left(\frac{-1.28\mathrm{eV}}{kT}\right)\varepsilon_{Si}kT}{D_{H^+}q} \qquad \text{(A2)}$$

can be defined.

The hydrogen molecule H_{2A} formation and dissociation is described by

$$\frac{d\left[H_{2A}\right]}{dt} = \left(-2.3\times10^{-6}\mathrm{cm}^3\mathrm{s}^{-1}\right)\exp\left(\frac{-1.3\mathrm{eV}}{kT}\right) \times \left(p\left[H_{2A}\right] - \frac{\left[H^+\right]\left[H^0\right]}{K_{H_{2A}}}\right) \qquad \text{(A3)}$$

with the equilibrium constant K_{H2A} for the atomic/molecular hydrogen

$$K_{H_{2A}} = \frac{p_d}{\chi_A}K^2. \qquad \text{(A4)}$$

Here, p_{d} signifies the hole concentration for the Fermi level coincident with the hydrogen donor level, and χ_{A} is the equilibrium constant for atomic hydrogen / HB pairs

$$\chi_A = \left(2.35\times10^{66}\mathrm{cm}^{-9}\right)\exp\left(\frac{-1.7\mathrm{eV}}{kT}\right). \qquad \text{(A5)}$$

Finally, the longterm decrease in the [HB]-concentration [51] is explained by the formation of a stable dimer H_{2C} with the reaction

$$\frac{d\left[H_{2C}\right]}{dt} = \left(5.5\times10^{11}\mathrm{s}^{-1}\right)\ \exp\left(\frac{-1.5\mathrm{eV}}{kT}\right) \times\left(\frac{\left[H^{+}\right]\left[HB\right]}{K} - \frac{\left[H_{2C}\right]\left[B^{-}\right]p^{2}}{5.25\times10^{51}\mathrm{cm}^{-9}}\right). \quad \text{(A6)}$$

B. Estimation of the LeTID Defect Concentration

We obtain a rough estimation in following three steps.

1) We transform the measured current values into effective carrier lifetimes τ_{eff}.

2) From these, we calculate the normalized defect densities N_t^*.

3) We calculate LeTID defect concentrations [*LD*] by a physically reasonable assumption of the electron capture cross section σ_{e} of the LeTID defect.

More precisely

1) A rough estimate of the effective carrier lifetime can be obtained from the measured currents at fixed applied bias by the equation [25]

$$R_{\text{cum}}\ (t) = \frac{\Delta n W}{\tau_{\text{eff}}\ (t)} = \frac{J_0\ (t)}{q}\ \frac{pn}{n_i^2} \quad \text{(B1)}$$

where R_{cum} signifies the cumulative carrier recombination in the entire depth *W* of the silicon wafer/solar cell, J_0 is the "recombination parameter" or dark saturation current and *q* the elementary charge. *p* and *n* indicate the hole and electron concentrations, respectively, n_i is the intrinsic carrier density, and $\tau_{\text{eff}}(t)$ indicates the effective carrier lifetime at time *t*. In (B1) it is assumed that the excess carrier density is distributed homogeneously along the depth. A second assumption is that $J_0(t)$ can be calculated from a simple one-diode model

$$J_0\ (t) = \frac{J\ (t)}{\exp\left(\frac{\mathrm{qV_a}}{\mathrm{kT}}\right) - 1} \quad \text{(B2)}$$

where V_a is the (series-resistance corrected) applied bias. Both assumptions are very crude, hence the effective carrier lifetime obtained by combining (B1) and (B2) is certainly affected by a large uncertainty.

2) Since the capture cross sections of the LeTID defect are not known, for quantification the normalized defect density N_t^* is often used as defined by

$$N_t^*\ (\Delta n) = \left(\frac{1}{\tau_{\text{eff}}\ (t,\Delta n)} - \frac{1}{\tau_{\text{eff},0}\ (\Delta n)}\right)^{-1} \quad \text{(B3)}$$

with $\tau_{\text{eff},0}$ being the initial carrier lifetime prior to degradation. As pointed out by Herguth [54], the normalized defect density depends on the excess carrier density. Therefore, we corrected the calculated N_t^* for Δn using the equations of [54] by assuming a mid-gap defect level with a capture cross section ratio of ∼30 [7], [39], [40].

3) Finally, we choose the absolute LeTID defect scale to match observations. We begin with an estimation of the minority carrier lifetime at low injection $\tau_{0\text{e}}$ in the fully degraded state of a heavily LeTID-affected sample. As demonstrated in [13] (see Fig. 5), $\tau_{0e} = 1/v_{th,e}\sigma_e[LD]$ can be as low as ∼20 μs in extreme cases. If this low value is caused by an active defect concentration of $[LD] = 1 \times 10^{11}$ cm^{-3}—which seems to be a reasonable order of magnitude—the electron capture cross section would be $\sim5\times10^{-14}$ cm^2, which is the same order of magnitude as for the most deleterious transition metals, such as Fe [41] or Cr [42]. With this value for σ_{e}, we calculate [*LD*] from $N_t^*{\sim}v_{th,e}\sigma_e[LD]$ at low injection.

References

[1] K. Ramspeck *et al.*, "Light induced degradation of rear passivated mc-Si solar cells," in *Proc. 27th Eur. Photovolt. Sol. Energy Conf. Exhib.*, 2012, pp. 861–865.

[2] A. Herguth and G. Hahn, "Kinetics of the boron-oxygen related defect in theory and experiment," *J. Appl. Phys.*, vol. 108, no. 11, 2010, Art. no. 114509.

[3] K. Krauss, A. A. Brand, F. Fertig, S. Rein, and J. Nekarda, "Fast regeneration processes to avoid light-induced degradation in multicrystalline silicon solar cells," *IEEE J. Photovolt.*, vol. 6, no. 6, pp. 1427–1431, Nov. 2016.

[4] R. Eberle, W. Kwapil, F. Schindler, M. C. Schubert, and S. W. Glunz, "Impact of the firing temperature profile on light induced degradation of multicrystalline silicon," *Phys. Status Solidi RRL*, vol. 10, no. 12, pp. 861–865, 2016.

[5] F. Kersten *et al.*, "System performance loss due to LeTID," *Energy Procedia*, vol. 124, pp. 540–546, 2017.

[6] D. Chen *et al.*, "Evidence of an identical firing-activated carrier-induced defect in monocrystalline and multicrystalline silicon," *Sol. Energy Mater. Sol. Cells*, vol. 172, pp. 293–300, 2017.

[7] F. Fertig *et al.*, "Mass production of p-type Cz silicon solar cells approaching average stable conversion efficiencies of 22%," *Energy Procedia*, vol. 124, pp. 338–345, 2017.

[8] H. C. Sio *et al.*, "Light and elevated temperature induced degradation in p-type and n-type cast-grown multicrystalline and mono-like silicon," *Sol. Energy Mater. Sol. Cells*, vol. 182, pp. 98–104, 2018.

[9] T. Niewelt *et al.*, "Light-induced activation and deactivation of bulk defects in boron-doped float-zone silicon," *J. Appl. Phys.*, vol. 121, no. 18, 2017, Art. no. 185702.

[10] D. Sperber, A. Heilemann, A. Herguth, and G. Hahn, "Temperature and light-induced changes in bulk and passivation quality of boron-doped float-zone silicon coated with SiNx:H," *IEEE J. Photovolt.*, vol. 7, no. 2, pp. 463–470, Mar. 2017.

[11] C. Renevier *et al.*, "Lifetime degradation on n-type wafers with boron-diffused and SiO_2/SiN-passivated surface," *Energy Procedia*, vol. 55, pp. 280–286, 2014.

[12] D. Chen *et al.*, "Hydrogen induced degradation: A possible mechanism for light- and elevated temperature-induced degradation in n-type silicon," *Sol. Energy Mater. Sol. Cells*, vol. 185, pp. 174–182, 2018.

[13] D. Chen *et al.*, "Hydrogen-induced degradation: Explaining the mechanism behind light- and elevated temperature-induced degradation in n- and p-type silicon," *Sol. Energy Mater. Sol. Cells*, vol. 207, 2020, Art. no. 110353.

[14] T. Luka, S. Großer, C. Hagendorf, K. Ramspeck, and M. Turek, "Intra-grain versus grain boundary degradation due to illumination and annealing behavior of multi-crystalline solar cells," *Sol. Energy Mater. Sol. Cells*, vol. 158, pp. 43–49, 2016.

[15] T. Luka, M. Turek, and C. Hagendorf, "Defect formation under high temperature dark-annealing compared to elevated temperature light soaking," *Sol. Energy Mater. Sol. Cells*, vol. 187, pp. 194–198, 2018.

[16] C. E. Chan *et al.*, "Rapid stabilization of high-performance multicrystalline p-type silicon PERC cells," *IEEE J. Photovolt.*, vol. 6, no. 6, pp. 1473–1479, Nov. 2016.

[17] S. Liu *et al.*, "Impact of dark annealing on the kinetics of light- and elevated-temperature-induced degradation," *IEEE J. Photovolt.*, vol. 8, no. 6, pp. 1494–1502, Nov. 2018.

[18] T. H. Fung *et al.*, "A four-state kinetic model for the carrier-induced degradation in multicrystalline silicon: Introducing the reservoir state," *Sol. Energy Mater. Sol. Cells*, vol. 184, pp. 48–56, 2018.

[19] F. Kersten *et al.*, "A new light induced volume degradation effect of mc-Si solar cells and modules," in *Proc. 31st Eur. Photovolt. Energy Conf.*, 2015, pp. 1830–1834.

[20] T. Niewelt *et al.*, "Understanding the light-induced degradation at elevated temperatures: Similarities between multicrystalline and floatzone p-type silicon," *Prog. Photovolt. Res. Appl.*, vol. 26, no. 8, pp. 533–542, 2018.

[21] D. Bredemeier, D. C. Walter, R. Heller, and J. Schmidt, "Impact of hydrogen-rich silicon nitride material properties on light-induced lifetime degradation in multicrystalline silicon," *Phys. Status Solidi RRL*, vol. 31, 2019, Art. no. 1900201.

[22] T. H. Fung *et al.*, "Impact of annealing on the formation and mitigation of carrier-induced defects in multi-crystalline silicon," *Energy Procedia*, vol. 124, pp. 726–733, 2017.

[23] T. H. Fung *et al.*, "Influence of bound hydrogen states on carrier-induced degradation in multi-crystalline silicon," *AIP Conf. Proc., 2018*, vol. 1999, 2018, Art. no. 130004.

[24] M. A. Jensen *et al.*, "Evaluating root cause: The distinct roles of hydrogen and firing in activating light- and elevated temperature-induced degradation," *J. Appl. Phys.*, vol. 124, no. 8, 2018, Art. no. 85701.

[25] U. Varshney *et al.*, "Evaluating the impact of SiN_x thickness on lifetime degradation in silicon," *IEEE J. Photovolt.*, vol. 9, no. 3, pp. 601–607, May 2019.

[26] A. C. N. Wenham *et al.*, "Hydrogen-induced degradation," in *Proc. IEEE 7th World Conf. Photovolt. Energy Convers. (A Joint Conf. 45th IEEE PVSC, 28th PVSEC & 34th EU PVSEC)*, Jun. 2018, pp. 1–8.

[27] V. V. Voronkov and R. Falster, "Formation, dissociation, and diffusion of various hydrogen dimers in silicon," *Phys. Stat. Sol. (b)*, vol. 254, no. 6, 2017, Art. no. 1600779.

[28] W. Kwapil, T. Niewelt, and M. C. Schubert, "Kinetics of carrier-induced degradation at elevated temperature in multicrystalline silicon solar cells," *Sol. Energy Mater. Sol. Cells*, vol. 173, pp. 80–84, 2017.

[29] A. Cuevas, "The recombination parameter J0," *Energy Procedia*, vol. 55, pp. 53–62, 2014.

[30] M. Selinger *et al.*, "Spatially resolved analysis of light induced degradation of multicrystalline PERC solar cells," *Energy Procedia*, vol. 92, pp. 867–872, 2016.

[31] S. Liu *et al.*, "Investigation of temperature and illumination dependencies of carrier-induced degradation in p-type multi-crystalline silicon," *AIP Conf. Proc.*, 2018, vol. 1999, Art. no. 130014.

[32] D. Bredemeier, D. C. Walter, and J. Schmidt, "Possible candidates for impurities in mc-Si wafers responsible for light-induced lifetime degradation and regeneration," *Sol. RRL*, vol. 2, no. 1, 2018, Art. no. 1700159.

[33] V. P. Markevich *et al.*, "Boron–oxygen complex responsible for light-induced degradation in silicon photovoltaic cells: A new insight into the problem," *Phys. Status Solidi A*, vol. 216, no. 17, 2019, Art. no. 1900315.

[34] D. Bredemeier, D. C. Walter, and J. Schmidt, "Light-induced lifetime degradation in high-performance multicrystalline silicon: Detailed kinetics of the defect activation," *Sol. Energy Mater. Sol. Cells*, vol. 173, pp. 2–5, 2017.

[35] C. Vargas Castrillon, G. Coletti, C. E. Chan, D. N. R. Payne, and Z. Hameiri, "On the impact of dark annealing and room temperature illumination on p-type multicrystalline silicon wafers," *Sol. Energy Mater. Sol. Cells*, vol. 189, pp. 166–174, 2019.

[36] T. R. Waite, "Theoretical treatment of the kinetics of diffusion-limited reactions," *Phys. Rev.*, vol. 107, no. 2, pp. 463–470, 1957.

[37] P. Pichler, *Intrinsic Point Defects, Impurities, and Their Diffusion in Silicon*, S. Selberherr, Ed. New York, NY, USA: Springer-Verlag, 2004.

[38] C. Chan *et al.*, "Modulation of carrier-induced defect kinetics in multi-crystalline silicon PERC cells through dark annealing," *Sol. RRL*, vol. 1, no. 2, 2017, Art. no. 1600028.

[39] P. G. Hamer *et al.*, "Modelling of hydrogen transport in silicon solar cell structures under equilibrium conditions," *J. Appl. Phys.*, vol. 123, no. 4, 2018, Art. no. 43108.

[40] B. J. Hallam *et al.*, "Development of advanced hydrogenation processes for silicon solar cells via an improved understanding of the behaviour of hydrogen in silicon," *Prog. Photovolt. Res. Appl.*, pp. 1–22, 2020.

[41] C. Herring, N. M. Johnson, and C. G. van de Walle, "Energy levels of isolated interstitial hydrogen in silicon," *Phys. Rev. B*, vol. 64, no. 12, 2001, Art. no. 125209.

[42] C. Q. Sun, F. E. Rougieux, and D. Macdonald, "A unified approach to modelling the charge state of monatomic hydrogen and other defects in crystalline silicon," *J. Appl. Phys.*, vol. 117, no. 4, 2015, Art. no. 45702.

[43] C. Vargas Castrillon *et al.*, "Carrier-induced degradation in multicrystalline silicon: Dependence on the silicon nitride passivation layer and hydrogen released during firing," *IEEE J. Photovolt.*, vol. 8, no. 2, pp. 413–420, Mar. 2018.

[44] D. C. Walter, D. Bredemeier, R. Falster, V. V. Voronkov, and J. Schmidt, "Easy-to-apply methodology to measure the hydrogen concentration in boron-doped crystalline silicon," *Sol. Energy Mater. Sol. Cells*, vol. 200, 2019, Art. no. 109970.

[45] T. Zundel and J. Weber, "Boron reactivation kinetics in hydrogenated silicon after annealing in the dark or under illumination," *Phys. Rev. B*, vol. 43, no. 5, pp. 4361–4372, 1991.

[46] K. Bonde Nielsen, B. Bech Nielsen, J. Hansen, E. Andersen, and J. U. Andersen, "Bond-centered hydrogen in silicon studied by in situ deep-level transient spectroscopy," *Phys. Rev. B*, vol. 60, no. 3, pp. 1716–1728, 1999.

[47] S. K. Estreicher, A. Docaj, M. B. Bebek, D. J. Backlund, and M. Stavola, "Hydrogen in C-rich Si and the diffusion of vacancy-H complexes," *Phys. Status Solidi A*, vol. 209, no. 10, pp. 1872–1879, 2012.

[48] A. Graf, A. Herguth, and G. Hahn, "Determination of BO-LID and LeTID related activation energies in Cz-Si and FZ-Si using constant injection conditions," *AIP Conf. Proc.*, vol. 2147, 2019, Art. no. 140003.

[49] S. A. McQuaid, M. J. Binns, R. C. Newman, E. C. Lightowlers, and J. B. Clegg, "Solubility of hydrogen in silicon at 1300°C," *Appl. Phys. Lett.*, vol. 62, no. 14, pp. 1612–1614, 1993.

[50] B. Hammann, J. Engelhardt, D. Sperber, A. Herguth, and G. Hahn, "Influencing light and elevated temperature induced degradation and surface-related degradation kinetics in float-zone silicon by varying the initial sample state," *IEEE J. Photovolt.*, vol. 10, no. 1, pp. 85–93, Jan. 2020.

[51] M. J. Binns, R. C. Newman, S. A. McQuaid, and E. C. Lightowlers, "Hydrogen solubility and defects in silicon," *MSF*, vol. 143–147, pp. 861–866, 1993.

[52] R. E. Pritchard, J. H. Tucker, R. C. Newman, and E. C. Lightowlers, "Hydrogen molecules in boron-doped crystalline silicon," *Semicond. Sci. Technol.*, vol. 14, no. 1, pp. 77–80, 1999.

[53] Y.V. Gorelkinskii and N. N. Nevinnyi, "EPR of interstitial hydrogen in silicon: Uniaxial stress experiments," *Mater. Sci. Eng., B*, vol. 36, no. 1–3, pp. 133–137, 1996.

[54] A. Herguth, "On the lifetime-equivalent defect density: Properties, application, and pitfalls," *IEEE J. Photovolt.*, vol. 9, no. 5, pp. 1182–1194, Sep. 2019.